



ELSEVIER

Biochimica et Biophysica Acta 1515 (2001) 83–91



www.bba-direct.com

Rapid report

Brownian dynamics study of an open-state KcsA potassium channel

T.W. Allen, S.H. Chung *

Department of Physics, Australian National University, Canberra, ACT 0200, Australia

Received 16 January 2001; received in revised form 11 July 2001; accepted 31 July 2001

Abstract

Three-dimensional Brownian dynamics simulations are used to study conductance of the KcsA potassium channel using the known crystallographic structure. Employing an open-state channel created by molecular dynamics simulations, current–voltage and current–concentration curves broadly consistent with experimental measurements are obtained. In the absence of an applied potential, the channel houses three potassium ions at positions that are in close agreement with X-ray diffraction maps. © 2001 Elsevier Science B.V. All rights reserved.

Keywords: Potassium channel; Molecular dynamics; Brownian dynamics; Conductance

The determination of the structure of the KcsA potassium channel from *Streptomyces lividans* has prompted numerous theoretical investigations [2–10] that have shed some light on mechanisms of permeation and selectivity within this important biological ion channel. In particular, molecular dynamics (MD) simulations have provided valuable structural information, ionic diffusion coefficients and thermodynamical analysis. While MD force-fields appear to mimic the ion positions found experimentally [1] over very short timescales [3,5], these experimental data have yet to be reproduced in a conducting channel. MD simulations with explicit channel protein and electrolyte solutions are, however, incapable of analyzing ion permeation for periods long enough to measure channel conductance ($\sim 1 \mu\text{s}$). To determine conductance in model channels, one-dimensional [11] and three-dimensional [12] Brownian dynamics (BD) simulations have been utilized. Recently simulations

on simplified potassium channels [13] have produced conductance data that is consistent with existing conductance measurements [14–16]. While this simplified model provides much insight into the physical mechanisms behind ion permeation in multi-ion channels, it is important that recent structural information be incorporated. Until now, no BD simulations have been carried out with the full experimentally-determined channel protein. Here, we demonstrate that a conducting state of the KcsA potassium channel can be generated with MD, such that the salient properties of this channel maybe reproduced with BD simulations. In carrying out such simulations, a possible structure and charge distribution for the KcsA open-state is developed, and a greater understanding of the permeation processes involved in this multi-ion channel is achieved.

Paramagnetic spin resonance studies [17,18], associated with the pH-dependent gating of this channel [14,19], have indicated that the experimental structure corresponds to a closed conduction state, and that the transmembrane helices, which form the intracellular pore, move away from the channel axis

* Corresponding author. Fax: +61-2-6247-2792.

E-mail address: shin-ho.chung@anu.edu.au (S.H. Chung).

during gating. We therefore increase the radius of the hydrophobic pore in a series of MD simulations to produce a conducting channel. BD simulations with this new open-state structure, that employ ionic diffusion estimates from previous MD simulations [10], are then used to study channel conduction. The protein structure of the KcsA channel [1] (PDB set *1bl8*) contains 396 residues or 3504 atoms, excluding polar hydrogens. The protein consists of four subunits, two of which are shown in Fig. 1A. Each subunit includes two transmembrane helices (inner and outer helices) forming the intracellular pore, a pore helix directed at a wide hydrophobic chamber, and a narrow selectivity filter protein. MD simulations with the CHARMM package [20] are performed using the CHARMM 19 extended atom parameter set, as detailed previously by Allen et al. [3]. The experimental protein structure is hydrated with SPC/E water molecules and attached to intracellular and extracellular reservoirs of water. Following heating to 298 K and 200 ps of equilibration, three K ions are placed near the experimentally determined positions [1] and held with $100 \text{ kT}/\text{\AA}^2$ harmonic constraints. Because an ion is seen to always reside near the intracellular entrance of the channel, we also place an ion in this region during molding. In a series of 100 ps MD simulations, atomic constraints of $20 \text{ kT}/\text{\AA}^2$ are applied to α -carbon atoms and target restraints are moved away from the channel axis until the minimum radius of the intracellular pore is $> 2.5 \text{ \AA}$. All restraints on the inner and outer helices are then removed such that transmembrane helices are free to rotate during a further 50 ps of simulation. Water molecules and ions are discarded and a single subunit is chosen, and replicated to impose 4-fold symmetry about the channel axis.

Three-dimensional BD simulations are used to predict the channel conductance and deduce the optimum charge on ionizable sidechains. In these simulations we solve the Langevin equation

$$m_i \frac{d\mathbf{v}_i}{dt} = -m_i \gamma_i \mathbf{v}_i + \mathbf{F}_i^R + q_i \mathbf{E}_i + \mathbf{F}_i^S, \quad (1)$$

where m_i , v_i , $m_i \gamma_i$ and q_i are the mass, velocity, friction coefficient and charge on an ion with index i , while \mathbf{F}_i^R , \mathbf{E}_i and \mathbf{F}_i^S are the random stochastic force, systematic electric field, and short ranged forces experienced by the ion, respectively. The Langevin

equation is solved with the algorithm of van Gunsteren et al. [21,22] using techniques described elsewhere [12,23,13]. A multiple timestep algorithm is used, where in the reservoirs a timestep of 100 fs is employed such that Eq. 1 becomes that of an overdamped oscillator (i.e., traditional Brownian dynamics), while in the channel a 2 fs timestep is employed such that the inertial term in Eq. 1 dominates, and the short-ranged interactions within the narrow pore are experienced by the ions. Electrostatic forces are determined by solving Poisson's equation with the boundary sector method [24], employing lookup table techniques [25,26]. Axial symmetry is imposed on the dielectric interface between water and protein. Protein atoms are assigned Born radii [27], and the channel pore is traced with a water molecule sphere of radius 1.4 \AA to determine the minimum boundary radius at each axial position. Because of the 4-fold symmetry of KcsA, and the large size of the water molecule used to trace the dielectric boundary, in comparison to the size of the KcsA pore, it is found that the axially symmetric boundary is a good approximation. Comparisons with non-axially symmetric boundaries, solved with a finite difference method [28], will be made to demonstrate this. Since the reservoirs in our system extend only a short way from the pore, it is the channel protein itself that is forming the dielectric boundary, and not a lipid bilayer. Thus the thickness of the low dielectric slab in Fig. 1A is $\sim 67 \text{ \AA}$, larger than that of a typical membrane. Bulk ionic diffusion coefficients ($1.96 \times 10^{-9} \text{ m}^2/\text{s}$ and $2.03 \times 10^{-9} \text{ m}^2/\text{s}$ for K and Cl ions, respectively [29]) are employed in reservoirs, but reduced values are used in the channel according to MD results [10]. Within the intracellular pore we maintain a bulk diffusion coefficient for the K ion, while a value of 50% bulk diffusion is employed in the chamber and selectivity filter regions. It is expected that the dielectric constant of channel water will be reduced somewhat from its bulk value of 80 [30]. In past simulations on a model KcsA channel [13], a value of 60 was seen to optimize conductance. However, the boundary sector method does not permit ions to cross dielectric boundaries. Therefore, we employ a dielectric constant of 60 throughout channel and bath water, and represent the change from reservoir (80) to channel water (60) by a Born energy barrier of $\sim 0.6 \text{ kT}$ (based on a Born radius of 1.93 \AA ,

determined from the enthalpy of hydration for K^+ ions [31]) erected at the channel entrances [13]. The dielectric constant of the protein is taken to be 2.

Short range forces we employ in the pore ($-25 \leq z \leq 25 \text{ \AA}$) include the Born energy barrier, an ion–ion interaction and a repulsive ion–protein inter-

action similar to that described by Chung et al. [13]. The ion–ion interaction consists of a long-ranged Coulomb term, and a short-ranged term that includes the influence of hydration waters which will have some bearing on relative ion positions within the channel. The K–K, K–Cl and Cl–Cl pair radial distribution functions reveal that there is a certain probability of ions being in contact, or being separated by one or more solvent molecules. The potentials of mean force for these ion pairs [34] can be given analytical forms [32,33]. When the Coulomb tail is subtracted, the ion–ion interaction becomes

$$U_{II}^{short} = U_o \left\{ \left(\frac{R_c}{r} \right)^9 - \exp[-(R-r)/c_e] \cos[2\pi(R-r)/c_w] \right\}, \quad (2)$$

where c_w is the oscillation length, c_e is the exponential drop parameter, R_c is the contact distance and R is the origin of the hydration force, each dependent on the particular ion pair. Simulations under various conditions, each lasting 0.5–1.0 μs , are performed with symmetric concentrations, generated with 16 K–Cl ion pairs in each reservoir. Reservoirs are of radius 30 \AA with height adjusted to set the desired concentration. With the exception of the current–concentration curves, 300 mM is used in all simulations, maintained with a stochastic boundary [13]. A transmembrane potential is generated by introducing an electric field into the solution of Poisson’s equation, as described previously [12].

BD simulations have been carried out with the

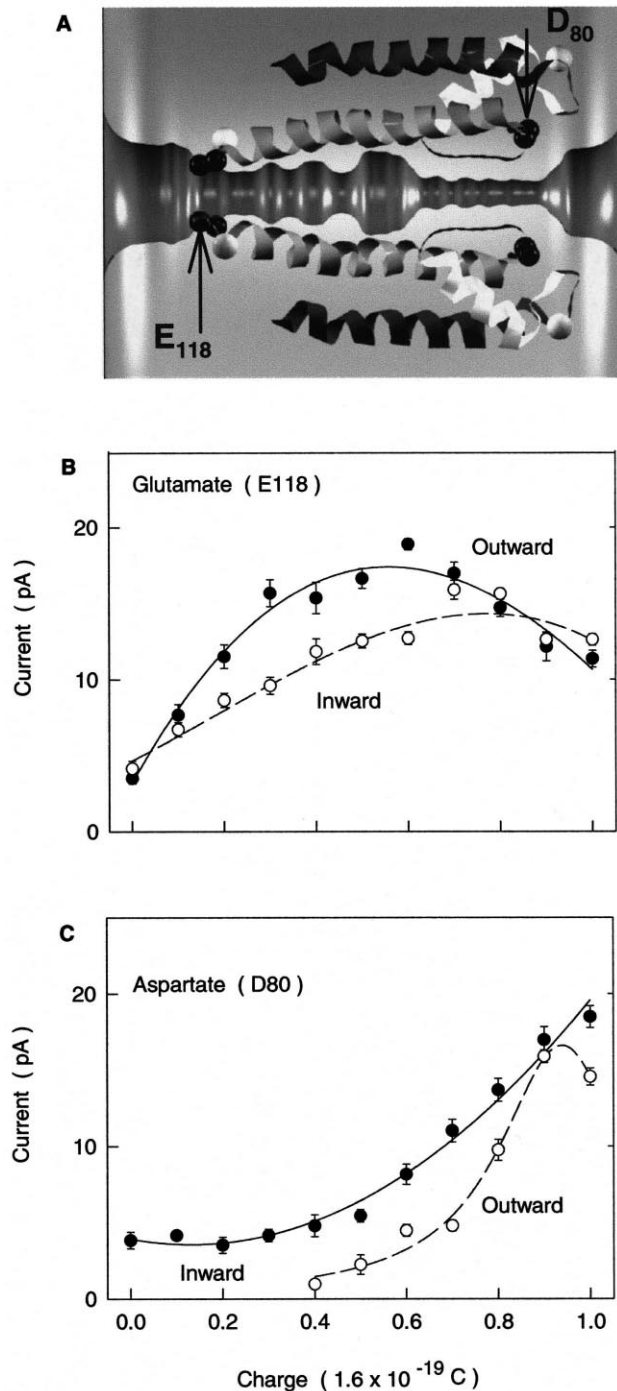


Fig. 1. Two of the four subunits of the KcsA channel are shown in A following molding with MD simulations. The dark gray, white, black and light gray ribbons represent the outer helices (approximate residues 23–61), pore helices (62–74), selectivity filter (75–79) and inner helices (80–119), respectively. The glutamic and aspartic acid (E₁₁₈ and D₈₀) carboxyl oxygen atoms are drawn as black spheres, while the arginine (R₁₁₇ and R₆₄) guanidine carbon atoms are drawn as light gray spheres. The boundary has an intracellular pore ($-23 \leq z < -4 \text{ \AA}$) with radius $\geq 2.7 \text{ \AA}$, reaching a maximum of 4.7 \AA in the chamber region ($-4 \leq z < 7 \text{ \AA}$), while that in the selectivity filter ($7 \leq z \leq 22 \text{ \AA}$) is $\geq 1.4 \text{ \AA}$. The variation in the outward (+247 mV, solid curve, filled circles) and inward (–269 mV, dashed curve, open circles) current with charges q_i and q_e on intracellular (B) and extracellular (C) mouth dipoles, respectively, is shown.

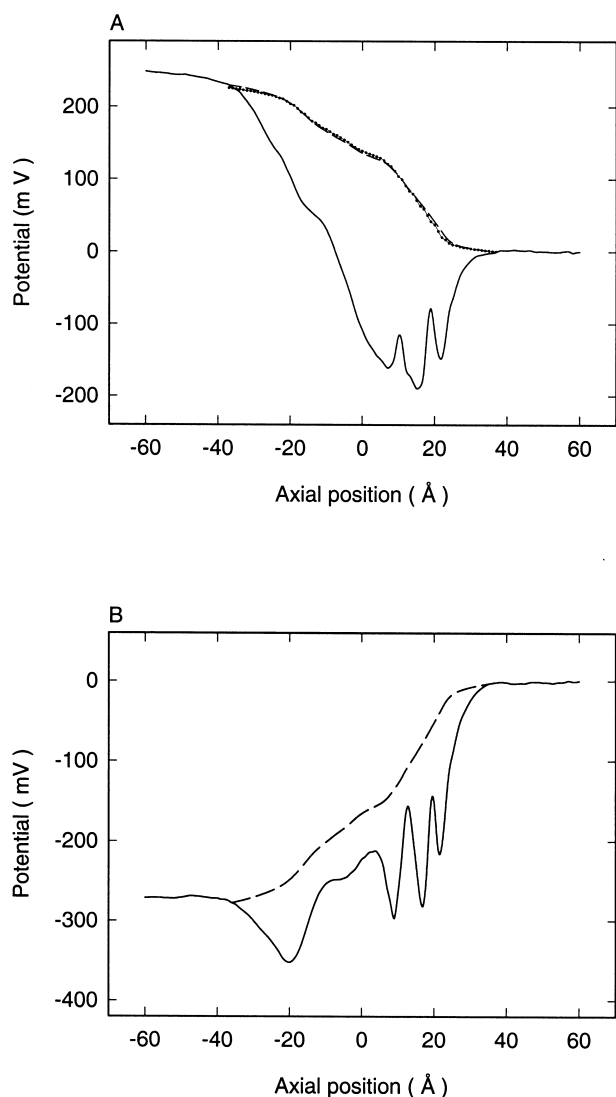


Fig. 2. The potential profile for an applied field of 2×10^7 V/m in the presence of all ions in the system and all protein charges (with $q_i = 0.3e$), averaged over a Brownian dynamics simulation, is shown as a solid curve in A. The potential profile across the channel with no ions present and all protein atomic charges set to zero is shown as a dashed curve. This potential has been scaled and shifted such that the potential at each reservoir entrance matches that found in the presence of all charges and ions. The potential profile for the same channel with a dielectric boundary which is not axially symmetric, but instead formed by generating the boundary with 36 angular divisions of 10° , is drawn as a dotted curve. This profile was calculated by solving Poisson's equation with a finite difference algorithm [28]. The potential profiles for an applied field of -2×10^7 V/m, with axially symmetric dielectric boundary, are shown in B.

extracellular entrance, and E₁₁₈ and R₁₁₇ near the intracellular entrance, require charge to enable conduction. The unpaired arginine R₂₇ near the intracellular pore, when charged, prevents conduction within this open-state model. It is likely that this residue could be neutralized by an acidic residue on the part of the transmembrane helices absent in the experimental coordinates. We find that charges on the distant E₅₁ and R₅₂ residues do not affect channel current significantly. Also, when charge is moved from the D₈₀ to the E₇₁ residue, changing the shape of the energy profile seen by an ion slightly, conduction almost ceases. Finally, since the presence of any net local charge severely hampers ion permeation, possibly due to the low dielectric strength of our protein, we consider only equal and opposite charges on acidic and arginine residues. Neutral and partially charged residues are created by distributing charge in a method based on the definitions of Lazaridis and Karplus [36].

We assign D₈₀ and R₆₄ charges $-q_e$ and $+q_e$, respectively, to create four extracellular mouth dipoles, and place charges $-q_i$ and $+q_i$ on E₁₁₈ and R₁₁₇ residues, respectively, to create four intracellular mouth dipoles. In Fig. 1B,C we show the variation in outward (filled circles) and inward (open circles) channel currents with charge on intracellular dipole q_i (Fig. 1B), and that with charge on extracellular dipole q_e (Fig. 1C). The potential difference is kept constant at +247 or -269 mV throughout, as determined below. The charge q_e is held constant at $0.9e$ during optimization of q_i , while q_i is fixed at $0.7e$ during optimization of q_e . When q_i is instead held

open-channel model of Fig. 1A with a range of charges on selected ionizable residues. Channels with wider intracellular pores, to be reported in a more detailed article, are seen to have substantially increased current. For example, a channel with a 4 Å radius pore has a conductance approximately double that observed experimentally. The open-channel model of Fig. 1A best approximates experimental conductance measurements, and is thus the obvious choice for this investigation. Each subunit of the KcsA protein consists of nine ionizable residues [1]. By investigating the effect of each of these charges on energy profiles and conduction, and by considering mutagenesis [35] and theoretical calculations [37,2,6], we have determined that only D₈₀ and R₆₄ near the

at $0.3e$ during optimization of q_e , very similar outward flowing currents are observed. Both outward and inward currents increase rapidly with intracellular charge q_i and remain high between $q_i = 0.3$ and $0.7e$. In contrast, the current reaches a maximum when the charge on the extracellular dipole q_e is near the full unit charge (e). From these results, we conclude that the values $0.9 \leq q_e \leq 1.0e$ and $0.3 \leq q_i \leq 0.7$ provide near optimal permeation in both directions. In the following simulations we consider two combinations of mouth dipoles. The first uses $q_i = 0.3$ and $q_e = 1.0e$, while the second uses $q_i = 0.7$ and $q_e = 0.9e$.

The effect of the dielectric boundary, protein atomic charges and ions on the potential profile for applied fields of 2×10^7 and -2×10^7 V/m is revealed in Fig. 2A,B, respectively. The time averaged potential profiles over a BD simulation at 300 mM, using $q_i = 0.3e$, are shown as solid curves. A potential profile at 1 Å steps, is taken at every 10 ps of a 10 ns simulation and averaged. The effect of ions is to leave a constant potential in the reservoirs, while the discrete ions lead to spikes in the selectivity filter region. The dielectric boundary and protein enhance the electric field such that when $+2$ mV/Å is applied, the potential difference measured across the centers of the reservoirs (± 50) is ~ 247 mV. When a field of -2 mV/Å is applied, the resulting potential difference is ~ -269 mV. Voltages reported throughout this article have been measured in this manner. The dashed curves in each graph correspond to a calculation of the potential profile with no ions present and all protein atomic charges set to zero, so as to reveal the influence of the boundary on the transmembrane potential. Because of the absence of ions

in the channel, the potential steps up across the channel in a smooth fashion. These profiles can be compared to existing Poisson–Boltzmann solutions [2] of the crystallographic and open model KcsA

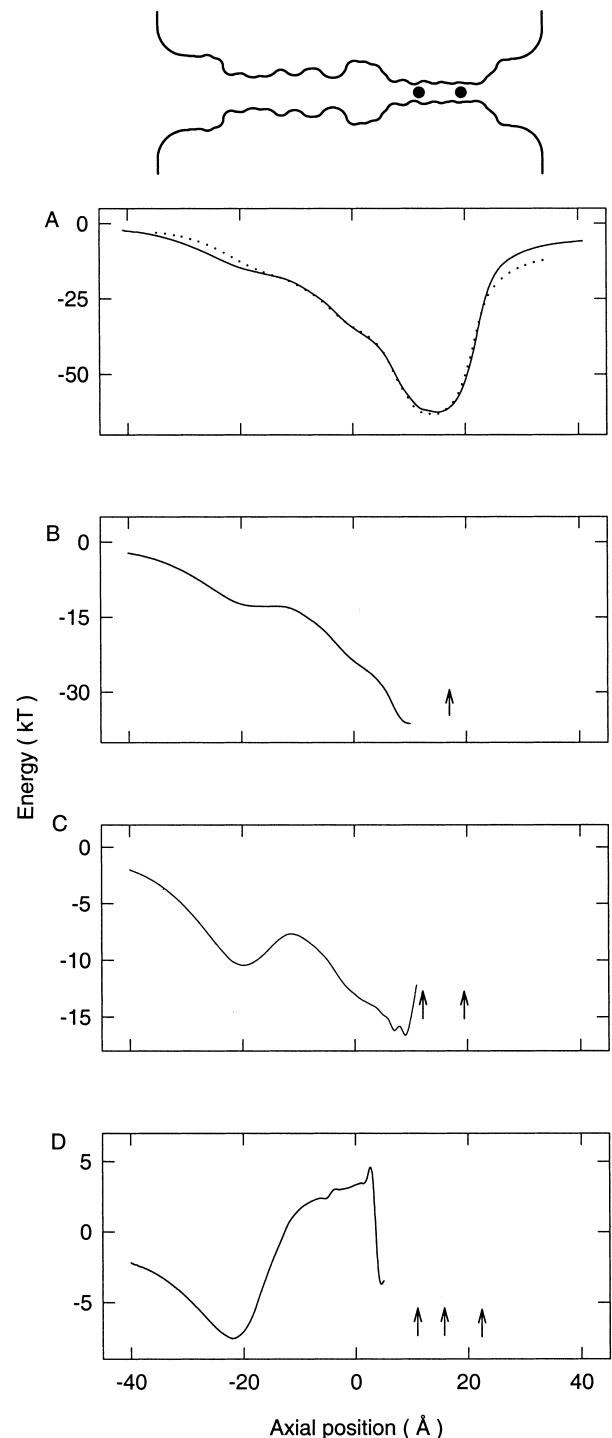


Fig. 3. The total electrostatic energy is plotted as a function of test ion position for a vacant channel in A. The solid and dotted curves correspond to axially symmetric and non-axially symmetric dielectric boundaries, respectively. Energy profiles with one, two and three ions resident in the selectivity filter-chamber region are shown in B–D, respectively. All calculations are performed in the presence of a $+247$ mV driving force, bringing an ion from the intracellular reservoir. Energies of multiple ion systems are calculated with a steepest descent algorithm [13]. The inset above the figures shows the shape of the dielectric boundary within the channel, aligned with the axes in the graphs, and a configuration of K ions representing the situation in C.

structures. The shapes of the curves are qualitatively similar, despite the fact that the channel model determined from molecular dynamics simulations in this work is likely to have a considerably different shape to that used previously [2]. We note that the profile in the reservoirs has not been shown for the dashed curves because it would simply be set to a constant value. A finite difference calculation of the potential profile with an asymmetric dielectric boundary formed by tracing the protein with a water molecule at 10° angular intervals, is shown as a dotted curve in Fig. 2A as a comparison. The profiles with symmetric and asymmetric dielectric boundaries are virtually indistinguishable. This reveals that the effect of axial symmetry on the transmembrane potential is negligible.

Fig. 3A shows the energy of a K ion brought into the channel from the intracellular reservoir in the absence of other ions for an axially symmetric dielectric boundary (solid curve). The charge on the intracellular dipole is fixed at $q_i = 0.3e$. Profiles with $q_i = 0.7e$ (not shown) are qualitatively similar. The energy well experienced by a single ion is ~ 60 kT deep within the selectivity filter with respect to the intracellular reservoir ($z = -50$). The dotted curve shows the energy profile found by solving Poisson's equation with a non-axially symmetric boundary with finite difference methods. The energy profiles with symmetric and asymmetric boundaries are very similar, with the exception of small differences near the reservoir entrances where the symmetric boundary has been rounded to provide a smooth interface for the boundary sector method solution. Again it is clear that the axially symmetric boundary is a reasonable approximation, and will be used in the remaining simulations. When one ion is positioned in the selectivity filter, a second ion entering the channel (Fig. 3B) still experiences a deep energy well of approximately 43 kT. With two ions residing in the selectivity filter, a third ion entering the channel (Fig. 3C) sees a small energy well created by mouth dipoles near the intracellular entrance, followed by a barrier of 4–5 kT as it moves toward the wide chamber region. The ion then experiences an energy minimum of approximately 17 kT in the wide cavity while two ions remain in the selectivity filter. This three-ion system is comparable in stability to that reported in existing atomic-detail calculations

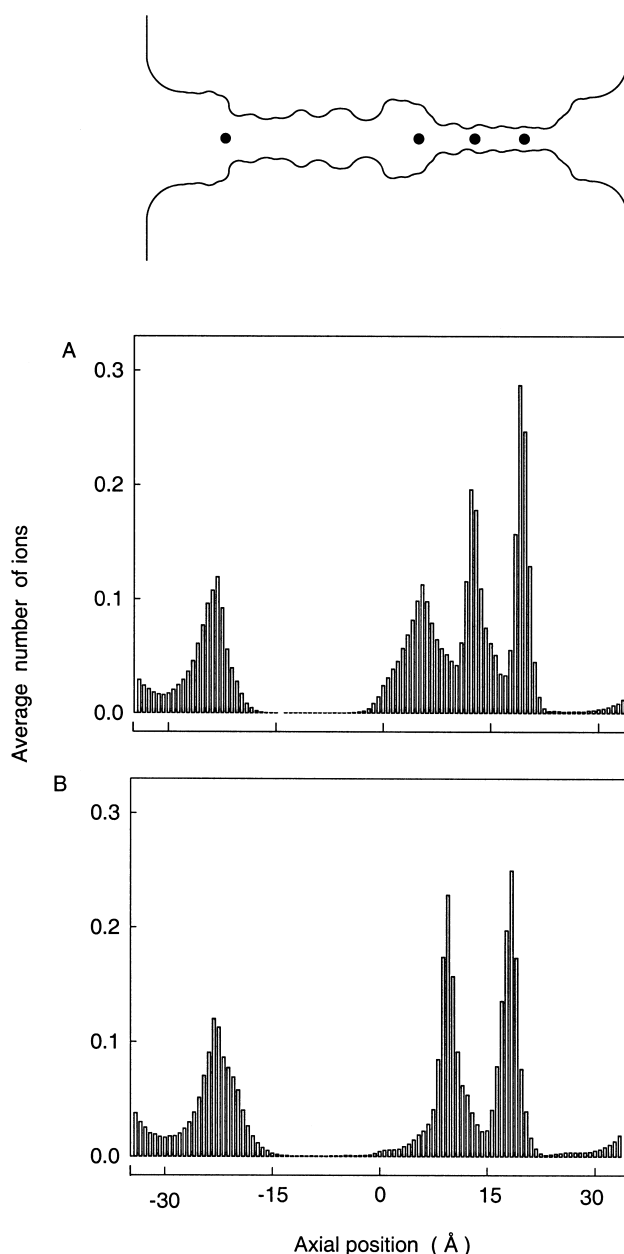


Fig. 4. Histogram revealing the mean location of ions, in the absence of any external potential (0 mV), for intracellular mouth dipole charge $q_i = 0.3e$ is shown in A. The histogram in the presence of a field driving ions from inside to outside of the cell (+247 mV) is shown in B.

[7]. A fourth ion entering the channel (Fig. 3D) sees a small energy well, and then a steeply rising energy barrier within the intracellular pore. The three-ion equilibrium is disrupted when the fourth ion enters the pore, expelling the outermost ion.

In Fig. 4 the channel is divided into 100 thin sections and the average number of ions over a 0.1 μs simulation is plotted. With no applied field, there are three prominent peaks in the histogram for $q_i = 0.3e$ (Fig. 4A). There are 2.9 ions in the selectivity filter and chamber and 1.0 ions in the intracellular entrance of the channel. The centers of the maxima are at -21.0 (near the E_{118} sidechain), 4.5 (inside the chamber), 12.3 (near the T_{75} carbonyl oxygen) and 19.2 Å (near the Y_{78} carbonyl oxygen), with a mean separation of ions of ~ 7.3 Å within the selectivity filter-chamber region. These positions are in close agreement with positions observed in X-ray diffraction maps [1]. The peaks in the histogram shift under the influence of an applied potential difference (shown for $q_i = 0.3e$ in Fig. 3C). There are two sharp peaks separated by 6.5 Å. On average, there are now 2.1 ions in the selectivity filter, indicating that the three-ion configuration in the chamber-selectivity filter segment is easily destabilized by an external field. We remark that when the charge q_i on E_{118} and R_{117} residues is increased from 0.3 to $0.7e$ (graphs not shown), the average number of ions near the intracellular mouth of the channel increases to ~ 2.0 , with only minor reorganization of ions within the selectivity filter and chamber regions.

In the presence of an outward driving external field, we provide a simplified analysis of the conduction events for $q_i = 0.3e$. The channel is divided into two halves such that ions in the chamber and filter sit on the right, while ions waiting near the intracellular mouth to cross the channel sit on the left. The default state of the channel in the presence of a $+247$ mV potential is [1,2]. Predominant conduction events are seen to consist of the following three transitions: [1, 2] \rightarrow [0, 3] \rightarrow [1, 3] \rightarrow [1, 2]. The ion waiting near the intracellular mouth overcomes the small barrier in the intracellular pore to enter the chamber region. Another ion enters the intracellular mouth while three ions reside in the channel. Because this system is unstable in the presence of an external field, the rightmost ion is ejected from the channel, leaving the system in its default configuration.

Fig. 5A,B display the current–voltage and current–concentration relationships respectively. The outward conductance at 140 mV is 35 pS, increasing to about 65 pS at 250 mV for both $q_i = 0.3e$ and $q_i = 0.7e$. The relationship is linear when the applied

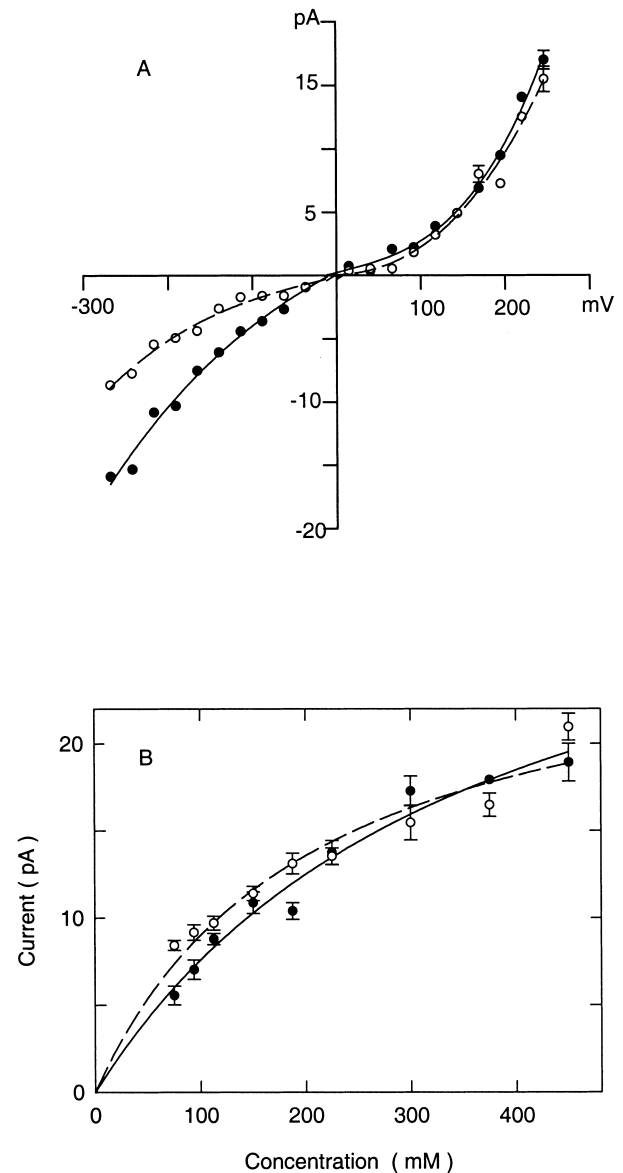


Fig. 5. The current–voltage curve (A) is generated using 300 mM solutions and fitted with a non-ohmic relationship described by Chung et al. [23]. The current–concentration curve (B) is generated with a voltage of $+247$ mV and fitted with a Michaelis–Menten equation [23]. The currents obtained with charges $q_i = 0.3$ and $0.7e$ are drawn with dashed curves (\circ) and solid curves (\bullet), respectively.

potential is less than about ± 140 mV but deviates from Ohm's law at a higher applied potential. This superlinearity in the current–voltage curve arises whenever the permeating ion must surmount an energy barrier, the degree of curvature depending on the barrier height [13]. In the curves illustrated here,

it can be seen that while the outward currents for intracellular dipole charge $q_i = 0.3$ and $0.7e$ are similar, significant attenuation of inward flowing current is observed with the smaller charge of $0.3e$. We remark that the KcsA channel is usually closed at neutral pH, but can remain in a conducting state at low intracellular pH [14,15]. Since the E_{118} sidechains are in close proximity to the cytoplasmic side of the membrane and accessible to channel water, they are subject to protonation at low pH. We conjecture that the open-state of the KcsA channel is likely to involve a reduced charge on the intracellular mouth dipole.

The conductances of the potassium channel we derive are in a broad agreement with those determined experimentally. There is some inconsistency between experimental conductance measurements, with studies reporting a dominant conductance substate of 90–97 pS [16,15], or as high as 135 pS (SKC1 from *Streptomyces lividans*) [19], while a study by Heginbotham et al. [14] reveals no substates and a lower outward conductance of 56 pS [14] (and inward conductance of 31 pS). Taking into consideration the differing concentrations and membrane potentials between electrophysiological measurements, and these simulations, the level of conductance and rectification observed in this model channel are consistent with experiment. The degree of rectification is also fairly inconsistent among experimental results [16,15,14]. Based on our comparison between $q_i = 0.3$ and $0.7e$, it seems likely that the charge on the intracellular mouth dipole may be varied so as to obtain the desired level of rectification.

The current saturates with an increasing ionic concentration, as shown in Fig. 5B. This arises because the ionic permeation across the channel is governed by two independent processes, one of which depends on the concentration and the other one that does not. With a potential difference of +247 mV, the time it takes for an ion to enter from the intracellular reservoir to the energy well near the channel entrance is 4.7 ns. This process is concentration-dependent. On the other hand, the time it takes for the ion in this energy well to surmount the barrier and proceed toward the selectivity filter is 5.9 ns. This time, being concentration-independent, becomes the rate-limiting step in conduction at high concentration. The current–concentration curves obtained with $q_i = 0.3e$ and

$q_i = 0.7e$ obey the Michaelis–Menten form, with the half saturation value of about 250 mM.

Employing a model of an open KcsA channel derived from MD simulations, comprehensive agreement with experimental conductance and X-ray diffraction results has been achieved. While there are some subtle differences in the shapes of the energy profiles throughout the selectivity filter and cavity in molecular [3] and Brownian dynamics (Fig. 3A), due to the different treatments of water and protein, both exhibit a deep energy well that usually holds three ions in the absence of a membrane potential. Time averages show that BD simulations lead to ion positions roughly in agreement with MD and experiment. The rigid protein and continuous dielectrics employed in BD are therefore yielding a reasonable approximation to the real interactions within this multiple ion channel.

The crystallographic structure, with narrow intracellular hydrophobic pore, need only be opened by 1–2 Å to achieve the high conductance observed experimentally. The charge on the glutamic acid residues lining the pore near the intracellular entrance must be reduced from the fully ionized form to $\leq 0.7e$, possibly by a decrease in electrolyte pH inside the cell, as seen experimentally [14], to allow the permeation of ions. A change in the protonation states of ionizable residues near the channel entrance is seen to lead to subtle differences in the shape of the current–voltage curve, current–concentration curve, and ionic distribution within the channel. Once accurate single channel conductance measurements become available, the results of these simulations can be used to select the most likely protonation states of these ionizable sidechains. Investigations into the combined effects of intracellular gate radius and ionizable residue protonation states are currently under way and will be reported elsewhere.

The success of this technique of using the full protein structure in MD and BD simulations has prompted studies of other ion channels including gramicidin A, porin and models of L-type calcium channels. It is hoped that similar predictions of channel dimensions and charge distributions can be made for these channels, and further insight into the mechanisms of ion permeation in ion channels can be obtained.

Acknowledgements

This work was supported by grants from the Australian Research Council and the National Health and Medical Research Council of Australia. All calculations were carried out with the Fujitsu VPP-300 of the ANU Supercomputer Facility. We thank Ben A. Corry for computing finite difference profiles with non-axially symmetric dielectric boundaries in Fig. 2A and 3A.

References

- [1] D.A. Doyle, J. Morais Cabral, R.A. Pfuetzner, A. Kuo, J.M. Gulbis, S.L. Cohen, B.T. Chait, R. MacKinnon, *Science* 280 (1998) 69–77.
- [2] B. Roux, S. Bernèche, W. Im, *Biochemistry* 39 (2000) 13295–13306.
- [3] T.W. Allen, A. Bliznyuk, A.P. Rendell, S. Kuyucak, S.-H. Chung, *J. Chem. Phys.* 112 (2000) 8191–8204.
- [4] T.W. Allen, S. Kuyucak, S.-H. Chung, *Biophys. J.* 77 (1999) 2502–2516.
- [5] J. Aqvist, V.B. Luzhkov, *Nature* 404 (2000) 881–884.
- [6] V.B. Luzhkov, J. Aqvist, *Biochim. Biophys. Acta* (2001) In press.
- [7] B. Roux, R. MacKinnon, *Science* 285 (1999) 100–102.
- [8] S. Bernèche, B. Roux, *Biophys. J.* 78 (2000) 2900–2917.
- [9] L. Guidoni, V. Torre, P. Carloni, *FEBS Lett.* 477 (2000) 37–42.
- [10] T.W. Allen, S.-H. Chung, S. Kuyucak, *Biophys. Chem.* 86 (2000) 1–14.
- [11] S. Bek, E. Jakobsson, *Biophys. J.* 66 (1994) 1028–1038.
- [12] S. Li, M. Hoyles, S. Kuyucak, S.-H. Chung, *Biophys. J.* 74 (1998) 37–47.
- [13] S.-H. Chung, T.W. Allen, M. Hoyles, S. Kuyucak, *Biophys. J.* 77 (1999) 2517–2533.
- [14] L. Heginbotham, M. LeMasurier, L. Kolmakova-Partensky, C. Miller, *J. Gen. Physiol.* 114 (1999) 551–559.
- [15] D. Meuser, H. Splitt, R. Wagner, H. Schrempf, *FEBS Lett.* 462 (1999) 447–452.
- [16] H. Schrempf, O. Schmidt, R. Kummerlin, S. Hunnah, D. Muller, M. Betzler, T. Steinkamp, R. Wagner, *Eur. Mol. Biol. Org. J.* 14 (1995) 5170–5178.
- [17] E. Perozo, D.M. Cortes, L.G. Cuello, *Nat. Struct. Biol.* 5 (1998) 459–469.
- [18] E. Perozo, D.M. Cortes, L.G. Cuello, *Science* 285 (1999) 73–78.
- [19] L.G. Cuello, J.J. Romero, D. Marien Cortes, E. Perozo, *Biochemistry* 37 (1998) 3229–3236.
- [20] B.R. Brooks, R.E. Bruccoleri, B.D. Olafson, D.J. States, S. Swaminathan, M. Karplus, *J. Comp. Chem.* 4 (1983) 187–217.
- [21] W.F. van Gunsteren, H.J.C. Berendsen, J.A. Rullmann, *Mol. Phys.* 44 (1981) 69–95.
- [22] W.F. van Gunsteren, H.J.C. Berendsen, *Mol. Phys.* 45 (1982) 637–647.
- [23] S.-H. Chung, M. Hoyles, T.W. Allen, S. Kuyucak, *Biophys. J.* 75 (1998) 793–809.
- [24] M. Hoyles, S. Kuyucak, S.-H. Chung, *Biophys. J.* 70 (1996) 1628–1642.
- [25] M. Hoyles, S. Kuyucak, S.-H. Chung, *Phys. Rev. E* 58 (1998) 3654–3661.
- [26] M. Hoyles, S. Kuyucak, S.-H. Chung, *Comput. Phys. Commun.* 115 (1998) 45–68.
- [27] M. Nina, D. Beglov, B. Roux, *J. Phys. Chem. B* 101 (1997) 5239–5248.
- [28] G. Moy, B. Corry, S. Kuyucak, S.-H. Chung, *Biophys. J.* 78 (2000) 2349–2363.
- [29] D.R. Lide (Ed.), *CRC Handbook of Chemistry and Physics*, CRC Press, Cleveland, OH, 1994.
- [30] M.S.P. Sansom, G.R. Smith, C. Adcock, P.C. Biggin, *Biophys. J.* 73 (1997) 2404–2415.
- [31] J.O'm. Bockris, A.K.N. Reddy, *Modern Electrochemistry*, Vol. 1, Plenum Press, New York, 1970.
- [32] E. Guàrdia, R. Rey, J.A. Padró, *Chem. Phys.* 155 (1991) 187–195.
- [33] E. Guàrdia, R. Rey, J.A. Padró, *J. Chem. Phys.* 95 (1991) 2823–2831.
- [34] B.M. Pettitt, P.J. Rossky, *J. Chem. Phys.* 84 (1986) 5836–5844.
- [35] L.G. Cuello, E. Perozo, *Biophys. J.* 78 (2000) 398A–398A.
- [36] T. Lazaridis, M. Karplus, *Proteins* 35 (1999) 133–152.
- [37] K.M. Ranatunga, I.H. Shrivastava, G.R. Smith, M.S.P. Sansom, *Biophys. J.* 80 (2001) 1210–1219.